LAWRENCE
LIVERMORE
NATIONAL
LABORATORY

LLNL-JRNL-421865

Investigating the possibility of a human component in various Pacific Decadal Oscillation indices

C. Bonfils and B. Santer

December 23, 2009

Climate Dynamics

Disclaimer

Physical Sciences: Environmental Sciences and Geophysics

Investigating the possibility of a human component in various Pacific Decadal Oscillation indices

Céline Bonfils*† and Benjamin Santer*

* Lawrence Livermore National Laboratory, Livermore, CA 94550, USA

Submitted to Proceedings of the National Academy of Sciences, December 22, 2009

† To whom correspondence should be addressed:
Email: bonfils2@llnl.gov, Phone: (925) 423 9923; Fax (925) 423 4908.

Manuscript information:
21 text pages (including title, abstract, references, figure legends and footnotes)
5 single column figures: (3.8+5.0+6.1+3.0+6.5)*180 = 4392
1 two-column figures: 9.0*360 = 3240

Word and character counts:
250 words in abstract
36279 characters in the text (with spaces)
43911 characters in total (including spaces and figures)

Abbreviations footnote: PDO, Pacific Decadal Oscillation; SST, Sea Surface Temperature; EOF, Empirical Orthogonal Function; S-PDOP, Spatial PDO Pattern; ERSST, Extended Reconstructed SST dataset; HadISST, Hadley Center Sea Ice and SST dataset; 20CEN, 20th century.

Author contributions: C.B. and B.S. designed research; C.B. and B.S. performed research; C.B. and B.S. analyzed data; and C.B. and B.S. wrote the paper.

Abstract: The Pacific Decadal Oscillation (PDO) is a mode of natural decadal climate variability typically defined as the principal component of North Pacific sea surface temperature (SST) anomalies. To remove any global warming signal present in the data, the traditional definition also specifies that monthly-mean, global-average SST anomalies are subtracted from the local anomalies. Because of this, any differences in the warming rates over the globe and the PDO region may be aliased into the PDO index itself. We examine the possibility of a human component in the PDO using three definitions. The implications of these definitions are explored using SSTs from both observations and model simulations of historical and future climate change, all projected onto definition-dependent observed PDO patterns. A systematic anthropogenic contamination is found in all PDO indices over the 21st century. Using the first definition—in which no warming signal is removed—the contamination is so large that it is statistically detectable in the observed PDO. Using the second (or traditional) definition, the contamination is large, arising mainly from the differential warming rates predicted in the North Pacific and globally. Removing the regional-mean signal (using the third definition) partially solves this problem, but a human signal persists because the predicted pattern of SST response to human forcing projects strongly onto the PDO mode. In consequence, statistically removing "natural variability" effects from a variety of observational datasets using PDO indices should be exercised with great caution. This illustrates the importance of separating internally-generated and externally-forced components in the PDO.

\body

Introduction

Climate indices provide a means of distilling complex patterns of spatio-temporal variability into simple forms. Indices such as the El Niño-Southern Oscillation (ENSO) or the Pacific Decadal Oscillation (PDO, 1-3) are often used to represent the behavior of modes of natural internal variability. Those modes of "unforced" variability share common features: they are thought to arise from interactions between the coupled atmosphere/ocean system; they display preferred spatial structures and can demonstrate sudden "regime shifts" or complex low-frequency behavior; and finally, evidence of such shifts or changes can be reconstructed from multi-century paleoclimate proxies (4) and captured in pre-industrial control simulations, in which time-varying external forcings are excluded (5, 6).

The PDO index is associated with the interdecadal variability of sea surface temperatures (SSTs) in the northern Pacific Ocean. It is distinguished by abrupt phase shifts (e.g., in 1925, 1947, and 1977), and can have a "far field" influence on climate through atmospheric teleconnections (7). A large variety of natural systems (*e.g.*, salmon productivity, drought-induced fires, annual river flow, onset of spring, *etc*...; 3, 8–10) and atmospheric variables have been related to the natural fluctuations in the PDO. Previous research studies (11–15) have employed these fluctuations to discover that climate variability alone cannot explain the declining snowpack, the decrease in snowfall fraction, and the earlier snowmelt runoff in the western U.S.

While knowledge of the current state of the PDO is recognized to be very valuable for seasonal and annual climate forecasts, for assessments of changes in natural systems (7, 16) and for decadal climate predictions (17), the physical mechanisms responsible for low-frequency behavior in the PDO are not yet fully understood (*e.g.*, 18, 19). Additionally, it is entirely

plausible that external forcings (e.g., greenhouse gas and sulfate aerosol forcing) have influenced north Pacific SSTs and the PDO index itself. Meehl *et al*. (20), for example, could only explain the prominent PDO regime change occurring in the mid-1970s by means of a combination of internally generated variability and anthropogenic forcing.

To date, the PDO index has primarily been defined in two different ways. Under the first definition, the PDO is the principal component of monthly SST anomalies in the Pacific Ocean poleward of 20ºN (*e.g*., 5, 3, 16, 14, 21, and many more). Under the second definition (the current "official" or "traditional" definition of the PDO[1]; 2, 7), monthly-mean global-average SST anomalies are first removed from local anomalies prior to calculation of principal components. The intent of this second index definition is to remove any externally forced "global warming" effect that may be present in the regional data (as illustrated in Fig. 1) and the PDO index itself. The implicit assumption in the official definition of the PDO is that any anthropogenically forced component of north Pacific SST variability can be removed by subtraction of the global-mean changes—i.e., that the SST response to anthropogenic forcing is spatially uniform. This assumption is unlikely to be true (22). Under this definition, any long-term, systematic difference in the warming rates of global-mean SST and SST in the PDO region will be aliased into the PDO index.

In this study, we investigate whether the PDO index contains a human signature. Our analysis considers both historical and projected future changes in SST in the PDO region. In the latter case, the imposed anthropogenic forcing is substantially larger than the estimated anthropogenic forcing over the 20th century, thus making it easier to separate forced and unforced SST variability. We examine the behavior of the PDO using: (1) a total of three definitions, (2) multiple observational SST datasets, (3) a suite of model simulations of 20th and 21st century climate change, and (4) selected multi-century unforced control runs.

Model and Observational Data

This work relies on three different observational SST datasets to estimate the spatial structure and temporal evolution of the PDO. The first one is from the U.K. Meteorological Office Hadley Center Sea Ice and SST dataset (HadISST, 23). The two others are versions 2 and 3 of the Extended Reconstructed SST dataset (ERSST2 and ERSST3, respectively; 24) of the National Oceanic and Atmospheric Administration. Our use of multiple datasets allows us to test the robustness of results to structural uncertainties in the observations. Model-based historical and future PDO indices are estimated using ensemble-average results from 17 different climate models. This set includes eight models (SELEC) that successfully capture key spatial and temporal characteristics of the PDO for the current climate (25)[2]. All 20th-century (20CEN) simulations include historical changes in various types of anthropogenic forcing. Half of them (and seven from the SELEC models) also include some form of solar and volcanic forcing. The 21st-century climate projections are based on the A2 scenario for future greenhouse gas and aerosol emissions. The results from the multi-model CMIP-3 archive supply valuable information on structural uncertainties in both the applied 20th and 21st century external forcings and the simulated climate response to these forcings[3]. Finally, multi-century preindustrial control (CTL) simulations performed with the SELEC models are used to compare historical and future PDO trends to those arising from internal climate variability alone. Further details of the models, forcings, and integrations are provided in the supporting information (SI) Text and Table S1.

PDO Definition

The official PDO (3) is based on "residual" monthly-mean SST anomalies in the North Pacific region, poleward of 20ºN. The residual anomalies are obtained for each grid point and for each month by: (1) removing the monthly climatology computed over the stipulated base period 1900–1993; and (2) subtracting the time-dependent global-mean SST anomaly for this particular month (see note #1). The dominant EOF of these residuals, calculated over the 94-year base period, is described as the observed "spatial PDO pattern" (S-PDOP). The full PDO time series for the entire analysis period is then obtained by projecting the residual anomalies onto the eigenvectors of 1900–1993-based S-PDOP. This procedure offers the advantage of a monthly update of the PDO time series with the option to switch to amended observational SST datasets (as done historically; see note #1 and SI Text) using the original S-PDOP and without modifying past PDO index values.

In here, we explore two alternatives to the "official" PDO definition (which we refer to here as "definition 2"). Definition 1 is a simplified version of the official PDO that does not involve any removal of a global-mean, monthly-mean SST signal prior to the EOF analysis. In definition 3, we subtract the regional-mean rather than the global-mean SST anomalies. The intent here is to avoid any aliasing of differences between warming rates over the North Pacific and the global oceans into the definition of the PDO. For each definition, we computed the leading EOF from the observed SST anomalies over 1900 to 1993 to estimate the spatial PDO patterns S-$PDOP_1$, S-$PDOP_2$, S-$PDOP_3$, respectively. This procedure yields nine different S-PDOP patterns (three observed SST datasets × three PDO definitions). For each dataset and definition, observed SST anomalies for the entire analysis period are then projected onto their corresponding S-PDOP, resulting in a total of nine observed PDO indices. Similarly, we projected the model SST anomalies (computed as specified in each definition) from the 20CEN, A2, and SELEC CTL integrations[4] onto their respective observed S-PDOP (see SI Text for more details). Since the

phasing of this internally generated component of the PDO is random in different realizations, the ensemble-averaging of SST anomalies over a sufficiently-large number of 20CEN and A2 realizations should help to reveal any underlying externally forced component in the PDO.

Observed PDO Patterns and PDO Time Series

The HadISST1-based S-PDOPs (Figs. 2a-c) capture the typical structural features of the spatial PDO pattern. A pool of anomalously cool water in the central North Pacific is surrounded by a horseshoe-shape stretch of anomalously warm waters (fixed, by convention, as the positive phase of the PDO). The intensity and the sign of the eigenvectors vary slightly with the index definition. This dominant mode explains ~27%, 30%, and 28% of the SST variance in the case of S-PDOP$_1$, S-PDOP$_2$ and S-PDOP$_3$, respectively. The weighted spatial average of the eigenvectors is negative for S-PDOP$_1$ and for S-PDOP$_2$, but (by definition) is zero in the case of S-PDOP$_3$ (see SI Table S2). This information will be important for understanding the sign of projected PDO trends.

The variability on the decadal time scale of the three observed PDO time series is large relative to changes in the PDO over the entire 20th century (Fig. 3a). As expected, PDO$_2$ correlates best with the official PDO index (r=0.93, see SI Table S2)[5]. The PDO$_1$ index shows a century-scale negative trend (-0.76 ± 0.43ºC/century) over the period 1900–2005 that is significantly different from zero (p=0.09)[6]. This trend arises from projecting a slow-evolving warming signal occurring in the PDO region (Fig. 1) onto the predominantly negative S-PDOP$_1$. Subtracting the time-evolving global mean SST changes (definition 2) yields, as anticipated, to the PDO$_2$ time-series with no overall statistically significant trend (0.17 ± 0.45ºC/century; p>0.5). The difference between the PDO$_2$ and PDO$_1$ indices (Fig. 3b) displays a clear century-time-scale positive trend and is highly correlated with the time-dependent globally averaged SST anomalies that are subtracted in definition 2 (r=0.99, D. Pierce, Pers. Comm.). This interdefinition difference is larger than differences arising from observational uncertainties of SST (as represented by horizontal lines in Figs. 3b).

Similarly, the differences between the PDO_3 and PDO_2 time-series are correlated with the differences between SST anomalies averaged over the PDO and global domains (r=0.76; Fig. 3b). Between 1900 and 1955, the PDO region has warmed more rapidly than the globe, with a statistically significant trend in the difference series over this period of +0.40°C/century ($p<0.001$). This produces a residual warming signal in the definition 2-computed SST anomalies that is projected onto the predominantly negative S-$PDOP_2$. Between 1955 and 1975, this dissimilarity in global and regional temperatures decreases, as does the difference between PDO_2 and PDO_3. Since the last PDO shift in 1977, the PDO region once again warms more than the globe, with a significant trend in the difference series (+0.76°C/century over 1978-2005, p=0.04), but this trend is not large enough to be inconsistent with climate noise (Fig. 4a; see SI Text). Overall, the interdefinition difference between PDO2 and PDO3 is not large enough to overcome the differences arising from observational uncertainties of SST. Results are qualitatively similar when using the ERSST datasets (see SI Text and Table S2). The only noticeable difference resides in the ERSST2-based PDO_1 trend, which is not large enough to be statistically different from zero.

Model-based Historical PDO Estimates

As in the observations, the PDO index inferred from individual 20CEN realization displays large decadal variability. Averaging over realizations and models reduces the internally generated noise, increases the signal-to-noise ratio, and highlights a possible PDO response to external forcing[7]. We examine here the PDO indices arising from the SELEC models (Fig. 3c).

As found in the observations, the multi-model average PDO_1 index shows a century-scale negative trend (-0.36±0.16 ºC/century over the period 1900-1999, p=0.03). The difference between the simulated PDO_2 and PDO_1 indices indicates a large century-long positive trend rising above observational uncertainties, highly correlated with the multi-model ensemble-mean globally-averaged SST anomalies (Fig. 3d). Interestingly, a large part of the variability of those

differences (and in the PDO_2 index itself) is in phase with fluctuations in the optical depth of stratospheric aerosols produced by massive volcanic eruptions[8]. This suggests that the use of definition 2 not only removes a global warming signal, it also makes the volcanic-induced signal apparent in the global-average SST time series more discernible in the PDO_2 index.

As in the observations, the difference time series between PDO_2 and PDO_3 correlates well with the differential warming rate existing between the PDO and the global domains (Fig. 3d). This differential warming rate does not, however, replicate all the fluctuations described in the observations until the end of the 1970s (Fig 3d). It is only after 1977 that the warming becomes faster in the PDO region than globally (as in the observations) in two-thirds of the 33 SELEC realizations (Fig. 4b). Nevertheless, using a Kolmogorov-Smirnov (KS) test, this distribution of 20CEN differential warming trends is not distinguishable from that arising from internally generated variability. (See SI Text for more details on the KS test.) All these results show qualitatively little sensitivity to the observational uncertainties and the set of models adopted (see SI Text, Figure S1 and Table S3).

Model-based Future PDO Estimates

For the A2 runs, the larger greenhouse gas forcing helps to highlight a possible PDO response to imposed human forcing (Figs. 3e-f). Indeed, one striking result is that *all* three PDO indices exhibit statistically significant century-scale negative trends over the 21st century. The origin of the trend differs for each index. In the case of the PDO_1 index, the large negative trend (-6.12±0.39ºC/century: $p<0.001$) arises mainly because the large anthropogenic warming in northern Pacific Ocean simulated in the A2 runs is projected onto the predominantly negative S-$PDOP_1$. In the case of the PDO_2 index, however, the trend (-2.00±0.22ºC/century, $p<0.001$) results from the rate of warming of the ocean surface simulated to be larger in the PDO region than globally[9] (Fig. 5), yielding to a residual SST warming projected onto the predominantly negative S-$PDOP_2$. In contrast with 20CEN-based results, the KS test indicates that this future

differential rate of warming domains cannot be explained by natural internal variability alone ($p<0.01$; Fig. 4c). Even under definition 3, a negative, statistically significant trend remains in the PDO_3 index (-1.18 ± 0.20 ºC/century, $p<0.01$). This trend arises from the modeled structural response of North Pacific SSTs to human forcing, predicting that the central pool of Northern Pacific will warm at a faster rate than along the U.S. coasts (Fig. 5). In projecting this slowly evolving cold-phase PDO-like spatial structure onto S-$PDOP_3$, a negative trend in PDO_3 appears. The multi-model averaged interdefinition differences (between PDO_1 and PDO_2 or between PDO_2 and PDO_3) are predicted to be large enough to easily overcome the current observational uncertainties (i.e., the horizontal lines in Fig. 3f). None of these results is very sensitive to observational uncertainties, or the set of models adopted (see SI Text, Figure S1 and Table S3)[10].

Comparison of Historical and Future PDO Trends with Unforced PDO Trends

To formally distinguish a slow-evolving externally-forced component in the PDO indices, we need to compare the century time-scale changes in the PDO seen in the observations, the historical and future climate change simulations relative to the century time-scale behavior of the PDO arising from natural internal climate variability alone. The methodology employed here consists of (1) comparing the distribution of 100-year 20CEN- and A2-derived PDO trends to the combined distribution of unforced PDO trends from overlapping 100-year CTL segments using a KS test, and (2) estimating the probability that the observed trends (from the three datasets) could be due to climate noise alone. This analysis is done for each definition independently (Fig. 6).

We found that the distribution of predicted future PDO trends and unforced PDO trends are statistically different at the 1% significance level, independent of the definition employed (Fig. 6). This means that the predicted PDO for the future cannot be explained by climate noise alone and are always anthropogenically contaminated in some ways (with a degree of influence that decreases from definition 1 to definition 3).

The distributions of 20CEN and unforced PDO trends are also found to be statistically different (at the 5% level), but only in the case of definition 1. Additionally, the HadISST1 and NOAA3 observed PDO_1 trends are found to be incompatible with changes arising from climate noise alone (at the 5% level, using a two-tailed test) but compatible with simulated historical changes. In contrast, for the two other definitions, the 20CEN and CTL distributions are not distinguishable, and the observed trends are compatible with both distributions.

Because the anthropogenic forcing has increased mainly at the end of the 20th century, we reiterated this analysis for a 22-year time scale period (See Fig S2 in SI). Again, none of the A2-derived 2078–2099 PDO trends can be explained by natural climate variability. This time, the distribution of 20CEN-derived 1978–1999 PDO trends is distinguishable from climate noise[11] (at the 5% level) not only for definition 1, but also for definition 2. However, none of the observed trends can be distinguished from the internally-generated variability, since the noise becomes too large compared to the signal on such a small time scale.

Summary and Concluding Remarks

In this study, we showed that the interpretation of changes in the PDO is problematic, and that the notion of representing the "natural" climate variability in the Pacific Ocean is challenged by human-induced global warming. If no global-mean SST signal is subtracted prior to the EOF analysis (our definition 1), the PDO index clearly includes a significant anthropogenically-forced component. This component is detectable at the century time scale in two of the three observed datasets, and in both historical and future model integrations. Thus, the observed PDO_1 does not represent a mode of variability that could be portrayed as entirely natural.

The official definition of the PDO (our "definition 2") makes the implicit assumption that any anthropogenic influence on PDO behavior is automatically removed by subtracting the time-

evolving changes in global-mean SST from local SST changes in the PDO region. We showed that this is unlikely to be the case. Differences in warming rates over the globe and in the PDO region start to appear at the end of the 20th century in two-third of the 20CEN runs and become both systematic and distinguishable from climate variability in the A2 simulations. Because of such differences, a residual anthropogenic signal is aliased into definition 2 of the PDO. The trends in simulated PDO_2 indices cannot be explained by climate variability from the end of the 1970s. The human component is, however, yet undetectable in the observed PDO_2 indices, which do not benefit from the signal-to-noise reduction technique (as do the multi-model ensemble simulations). Signs of failure of this "official" definition should appear in the future as the spatial heterogeneity in North Pacific SST responses to anthropogenic forcing amplifies, and the likelihood of a more rapid warming in extratropical regions increases.

To minimize the "contamination" of the PDO by direct or residual anthropogenic warming, we subtracted the time-evolving changes in regional SST from local SST changes prior the EOF analysis (our definition 3). In this last case, the anthropogenic contamination in PDO_3 is much slower and associated with the structural warming response of SSTs in the PDO region (Fig. 5). The patterns of SST response to greenhouse gas forcings present spatial features similar to the spatial PDO pattern, and thus project strongly onto the natural PDO mode of variability. This yields to a negative trend in the PDO_3 index that is only distinguishable for climate variability in the A2-based PDO_3 time-series. This feeds the debate (e.g.: 26–30) on the possibility that response to human activity may manifest itself in natural climatic modes by changing frequency of occurrence, or in shifting the natural fluctuations to spin around new attractors (31).

Our results corroborate previous research (25) that suggests that the variability in North Pacific SST will be dominated by a warming trend rather than by PDO variability. But our results also suggest that on top of the overall warming of North Pacific, a warmer central North Pacific (relatively to the coast) will be favored in response to anthropogenic forcings. Our study

illustrates that North Pacific SST changes over the 20th and 21st centuries have both internally-generated and externally-forced components, and that the strengths of these components are highly dependent on the definition employed. Understanding both components is important in improving the decadal predictability of future changes in regional climate, droughts, and natural systems. Since the PDO is often used to statistically remove "natural variability" effects from a variety of observational datasets, such noise removal exercises should be exercised with great care.

Acknowledgments

We thank the international modeling groups for providing their data for the analysis, the Program for Climate Model Diagnosis and Intercomparison for collecting and archiving them, and the World Climate Research Program's Working Group on Coupled Modeling for organizing the model data analysis activity. We warmly thank David Pierce and Tim Barnett for their helpful comments, notably in the origin of the interdefinition differences. This work was performed under the auspices of the U.S. Department of Energy by Lawrence Livermore National Laboratory under Contract DE-AC52-07NA27344. A portion of this study was supported by the US Department of Energy, Office of Biological and Environment Research.

[1] The official definition can be found at http://jisao.washington.edu/pdo/PDO.latest.
[2] Different performance tests (17, 18, 21) could have led to a slightly different set of selected models.
[3] Multi 20CEN (A2) realizations exist for 13 (7) of the 17 models analyzed here. The realizations from a particular ensemble contain identical changes in external forcings but differ only in their initial conditions. This approach yields many different realizations of the climate "signal" (the response to the imposed forcing changes) plus climate noise.
[4] SST anomalies from A2 simulations have been constructed relative to the seasonal climatology over the period January 2000 December 2009. The climatology used for the CTL runs have calculated over the 10 first years of the integrations.
[5] These two time-series are however not perfectly identical owing to the differences in the datasets, adopted horizontal resolution, and strategies chosen for global mean calculation and sea-ice treatment. For instance, in January 2002, the SST dataset used to calculate the official PDO index has changed (see http://jisao.washington.edu/pdo/PDO.latest)
[6] PDO_1 ends up predominantly in cold phase because the time-series have been plotted relatively to the period 1900-1909 for figure clarity.

[7] In theory, a mode of variability that is entirely natural should fluctuate around zero and produce, with a large enough number of weather noise realizations, a zero average and no trend.
[8] Five of these volcanic events also coincide with a dip in the observed difference time-series (Fig. 3b).
[9] as seen at end of the 20th century in observations and two-third of the 20CEN simulations.
[10] The amplitude of the PDO_1 trend is however sensitive to the base period employed for anomaly definition (see SI Text and Figure S3).
[11] Define as the combined unforced trends distribution from a series of 22-year long SELECT CTL run segments.

References

1. Hare SR (1996) Low Frequency Climate Variability and Salmon Production. A Dissertation by SR Hare submitted in partial fulfillment of the requirements for the degree of Doctor of Philosophy University of Washington 1996.

2. Zhang Y, Wallace J.M, Battisti DS (1997) ENSO-like interdecadal variability: 1900–93's. *J Clim* 10:1004–1020.

3. Mantua N, Hare S, Zhang Y, Wallace J, Francis R (1997) A Pacific interdecadal oscillation with impacts on salmon production. *Bull Am Met Soc* 58:1069–1079.

4. Biondi F, Gershunov A, Cayan DR (2001) North Pacific decadal climate variability since AD 1661. *J Clim* 14:5–10.

5. Hunt BG (2008) Secular variation of the Pacific Decadal Oscillation, the North Pacific Oscillation and climatic jumps in a multi-millennial simulation. *Clim Dyn* 30:467–483.

6. Pierce DW, Barnett TP, Latif M (2000) Connections between the Pacific Ocean tropics and midlatitudes on decadal time scales. *J Clim* 13:1173–1194.

7. Mantua N, Hare S (2002) The Pacific decadal oscillation. *J Oceanogr* 58:35–44.

8. Schoennagel T, Veblen TT, Romme WH, Sibold JS, Cook ER (2005) ENSO and PDO variability affect drought-induced fire occurrence in Rocky Mountain Subalpine forests. *Ecol Appl* 15:2000–2014.

9. Neal EG, Walter MT, Coffeen C (2002) Linking the pacific decadal oscillation to seasonal stream discharge patterns in Southeast Alaska. *J Hydrol* 263:188–197.

10. Cayan DR, Kammerdiener SA, Dettinger MD, Caprio JM, Peterson DH (2001) Changes in the onset of spring in the western United States. *Bull Amer Meteor Soc* 82:399–415.

11. Mote PW (2003) Trends in snow water equivalent in the Pacific Northwest and their climatic cuases Declining mountain snowpack in western North America. *Geoph Res Lett 1601, doi:10.1029/2003GL017258.*

12. Knowles N, Dettinger MD, Cayan DR (2006) Trends in Snowfall versus Rainfall in the Western United States. *J Clim* 19:4545–4559.

13. Stewart IT, Cayan DR, Dettinger MD (2005) Changes to earlier streamflow timing across Western North America. *J Clim* 18:1136–1155.

14. Pierce, DW, Barnett TP, Hidalgo GH, Das T, Bonfils C, Santer BD, et al. (2008) Attribution of Declining Western U.S. Snowpack to Human Effects. *J Clim* 21:6425–6444.

15. Bonfils C, Santer BD, Pierce DW, Hidalgo HG, Bala G, et al. (2008) Detection and Attribution of Temperature Changes in the Mountainous Western United States. *J Clim* 21:6404–6424.

16. McCabe GJ, Dettinger MD (2002) Primary modes and predictability of year-to-year snowpack variations in the western United States from teleconnections with Pacific Ocean climate. *J Hydrometeorol* 3:13– 25.

17. Latif M, Barnett TP (1996) Decadal climate variability over the North Pacific and North America: Dynamics and predictability. *J Clim*, 9:2407-2423.

18. Nakamura, H., G. Lin, and T. Yamagata, 1997: Decadal climate variability in the North Pacific during the recent decades. *Bull Amer Meteor Soc,* **78,** 2215–2225.

19. Trenberth KE, Hurrell JW (1994) Decadal atmosphere—ocean variations in the Pacific. *Clim Dyn* 9:303–319.

20. Meehl GA, Hu A, Santer BD (2009) The mid-1970s climate shift in the Pacific and the relative roles of forced versus inherent decadal variability. *J Clim*, in press.

21. Sun J, Wang H (2006) Relationship between Arctic Oscillation and Pacific Decadal Oscillation on decadal timescale. *Chin Sc Bull* 51:75–79.

22. Meehl GA *et al*. *Global Climate Projections*, in *Climate Change 2007: The Physical Science Basis, Contribution of Working Group I to the Fourth Assessment Report of the Intergovernmental Panel on Climate Change*, S. Solomon *et al.* Eds. (Cambridge Univ. Press, Cambridge, 2007).

23. Rayner NA, Brohan P, Parker DE, Folland CK, Kennedy J, et al. (2006) Improved analyses of changes and uncertainties in sea surface temperature measured *in situ* since the mid nineteenth century. *J Clim* 19:446–469.

24. Smith, TM, Reynolds RW (2004) Improved extended reconstruction of SST (1854-1997). *J. Clim* 17:2466–2477.

25. Overland JE, Wang M (2007) Future Climate of the North Pacific Ocean. *Eos, transactions Am Geoph Union*, 88:178–182.

26. Corti S, Molteni F, Palmer TN (1999) Signature of recent climate change in frequencies of natural atmospheric circulation regimes. *Nature* 398:799–802.

27. Fedorov AV, Philander SG (2000) Is El Niño Changing? *Science* 288:1997– 2002.

28. Shindell DT, Miller RL, Schmidt GA, Pandolfo L (1999) Simulation of recent northern winter climate trends by greenhouse-gas forcing. *Nature* 399:452–455.

29. Timmermann A, Oberhuber J, Bacher A, Esch M, Latif M, Roeckner E (1999) Increased El Nino frequency in a climate model forced by future greenhouse warming. *Nature* 398:694–697.

30. Cubash U, GA Meehl, GJ Boer, RJ Stouffer, M Dix, A Noda, CA Senior, S Raper and KS Yap, (2001) Projections of future climate change. Chapt. 9 In: J. Houghton et al. Editors, Climate Change 2001. The Scientific Basis. Intergovernmental Panel on Climate Change, Cambridge University Press.

31. Palmer T (2008) Introduction in CLIVAR Exchanges - Natural Modes of Variability under Anthropogenic Climate Change. Southampton, UK, International CLIVAR Project Office, 32pp. (CLIVAR Exchanges, No. 46 (Vol.13 No.3) (available at http://eprints.soton.ac.uk/55670).

32. Sato M, Hansen JE, Lacis A, McCormick MP, Pollack JB (1993) Aerosol optical depths, 1850-1990, *J Geophys Res* 98:22987–22994.

Figure Legends

Fig. 1: Observed time series of annual mean, spatially averaged SST anomalies in the PDO region (245-115ºW, 20-60ºN) from HAdISST1, ERSST2 and ERSST3 regridded datasets. All SST anomalies are defined relative to climatological monthly means over 1900 through 1909. The reference period was chosen for visual display purposes only. All trends (in ºC/century), calculated over the period 1900–2005, are significantly different from zero at the 1% level ($p<0.01$). The vertical line indicates the year during which the official PDO index has been developed.

Fig. 2: Leading EOF pattern of the North Pacific SST residuals (i.e., spatial PDO patterns) obtained from: A. definition 1 (simple SST anomalies prior the EOF analysis; S-PDOP$_1$); B. definition 2 (global mean SST removed; S-PDOP$_2$); and C. definition 3 (regional mean SST removed; S-PDOP$_3$); D. Second leading EOF pattern obtained from definition 1. All EOFs are based on HadISST1 dataset and the base period 1900–1993 (as in the official definition).

Fig. 3: A. Observed annual mean PDO$_1$, PDO$_2$, and PDO$_3$ time-series projected onto their respective S-PDOP (in Figs. 2a-c) using the HadISST1 dataset. B. Difference between the two observed time-series PDO$_2$ and PDO$_1$ (thick brown line) and PDO$_3$ and PDO$_2$ (thick pink line). They correlate with the annual mean, globally-averaged SST anomalies time-series (thin brown line) and the difference between SST anomalies averaged over the globe and the PDO region (thin pink line). C. Same as A. but for the average of the 8 selected 20CEN ensembles projected

onto their corresponding observed S-PDOP. The grey, orange and green envelops are the 1σ confidence intervals for the simulated PDO_1, PDO_2 and PDO_3. D. Same as B. but for the average of the 8 20CEN ensembles. The grey envelops are the 1σ confidence intervals for the PDO differences time series. E. and F. Same as C. and D. but for the average of the 8 A2 ensembles projected onto their respective observed S-PDOP. All SST anomalies that are projected are defined relative to climatological monthly means over 1900 through 1909 for the historical period and over 2000 through 2009 for the future period. The reference period was chosen for visual display purposes only. It has no impact on trend analyses but may change the partition of cool and warm phases, especially for the observed and simulated historical period. The filled blue time-series is the observed changes in estimate of stratospheric aerosol optical depth (SAOD, 32). Dotted lines denote the times of maximum SAOD during major volcanic eruptions. The dashed horizontal lines in B, D, and F is a measure of observational uncertainties represented as the 1 temporal standard deviation from the difference between the HadISST1 and ERSTT2 PDO_3 time series. These observational uncertainties arise from both sparse data coverage and from the different reconstruction procedures used to infill missing SST data.

Fig. 4: Comparison between observed and simulated trends in differential warming between the PDO and global domains (in °C/century) on the 22-year time scale. Observed and simulated historical trends are computed over the period 1978–1999, while future trends are calculated over the period 2078–2099. Sampling distribution of unforced trends was obtained from a total of 744 nonoverlapping 22-year segments of the CTL integrations. Sampling distributions of simulated historical (future) trends was obtained from the 33 (23) SELEC 20CEN (A2) realizations. The three lines indicate observed trends in the HadISST1 and the ERSSTs data. A KS test indicates the distribution of A2 trends is statistically different (at the 5% significance level) from that generated from internally generated variability. This is not the case with the 20CEN distribution.

The observed trends are not large enough to be inconsistent with climate noise (see SI Text). Note that similar results are obtained for the periods 2070–1999 and 2075–1999.

Fig. 5: A. Multi-ensemble average of SST trends over the period 2001–2099 (in ºC/decade) using the SELEC models (See Fig. S4 in SI for a more detailed analysis of 1900–1999 and 2001–2009 simulated trends).

Fig. 6: Comparison between observed and simulated trends in PDO indices on the century time scale for definition 1 (panel A), 2 (panel B) and 3 (panel C). Here, all PDO indices obtained using the three different observational datasets are included, to account for observational uncertainties. Observed and simulated historical trends are computed over the period 1900–1999, while future trends are calculated over the period 2001–2099. Sampling distribution of unforced trends was obtained from a total of 3×744 nonoverlapping 100-year segments of the CTL integrations. Sampling distributions of simulated historical (future) trends was obtained from the 3×33 (3×23) SELEC 20CEN (A2) realizations. The three lines indicate observed trends in the HadISST1 and the ERSSTs data.

Fig. 1

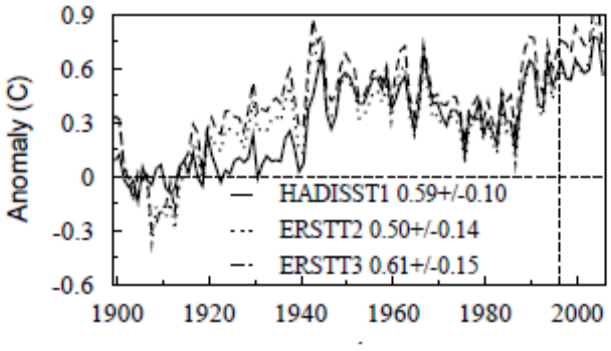

Fig. 2

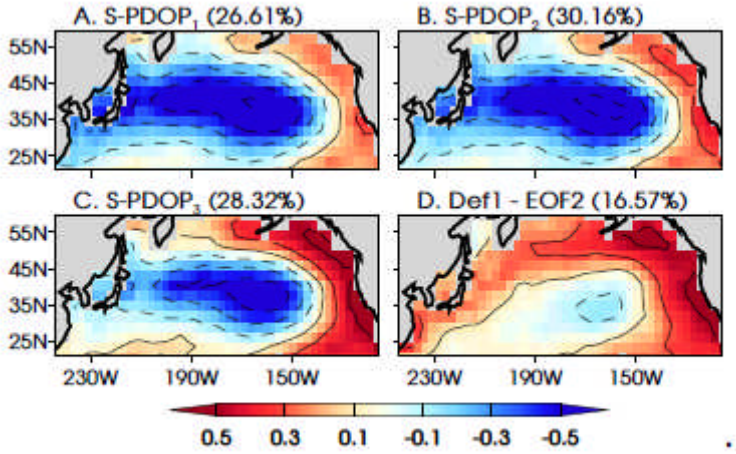

Fig. 3

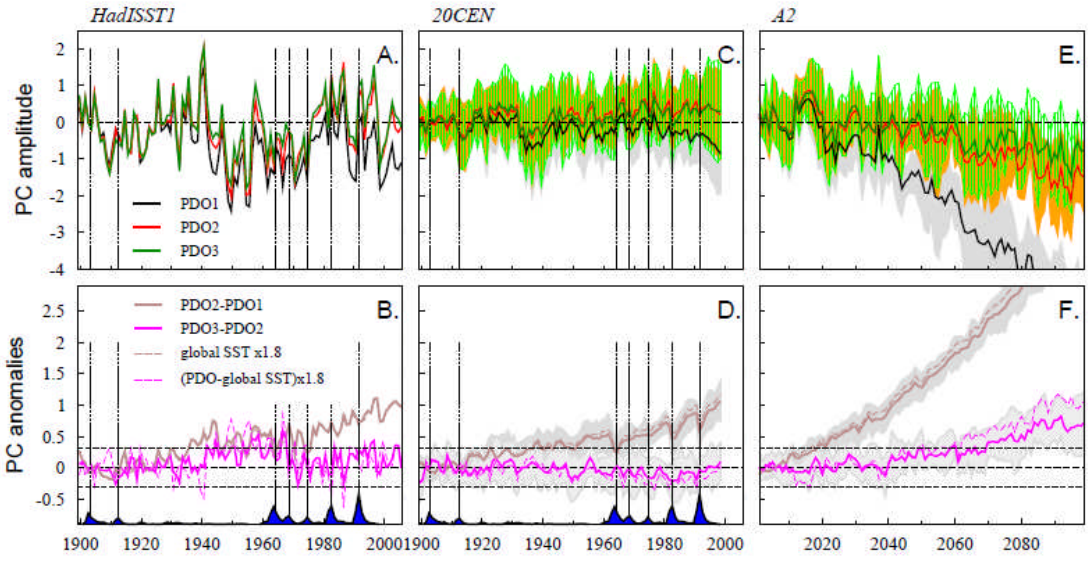

Fig. 4

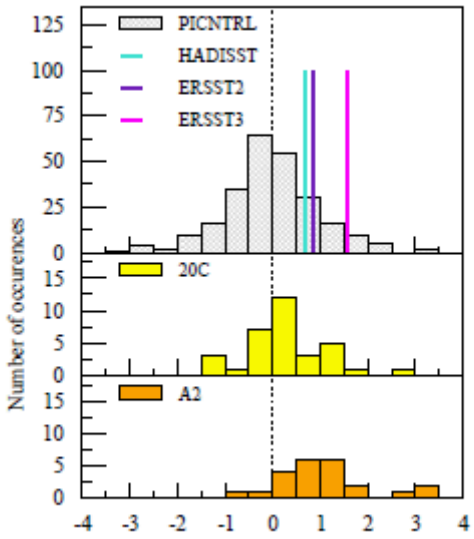
PICNTRL
HADISST
ERSST2
ERSST3
20C
A2
Number of occurences
125
100
75
50
25
0
15
10
5
0
15
10
5
0
-4
-3
-2
-1
0
1
2
3
4

Fig. 5

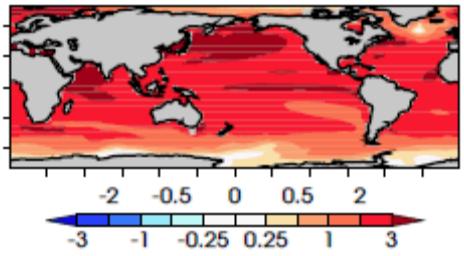
-2
-0.5
0
0.5
2
-3
-1
-0.25
0.25
1
3

Fig. 6

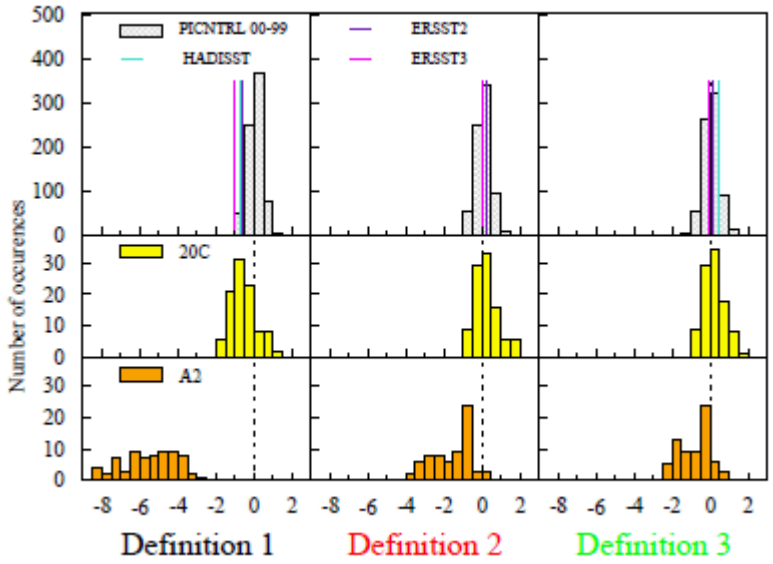

Supporting Text

1. Observational sea surface temperatures (SSTs)

We used versions 2 and 3 of the National Oceanographic and Atmospheric Administration Extended Reconstructed SST dataset (ERSST2 and ERSST3, respectively; S1) and the Hadley Center Sea Ice and SST dataset (HadISST, S2). The datasets are in the form of monthly mean data, spanning from January 1880 to December 2005 for ERSST2, January 1854 to December 2006 for ERSST3, and January 1870 to December 2006 for HadISST. ERSSTs and HadISST1 datasets are provided on a 2ºx2º and 1ºx1º latitude/longitude grids, respectively. Reconstruction of SST anomalies involved a fitting to a set of spatial modes in ERSST datasets, and a two-stage reduced-space optimal interpolation procedure in HadISST1 dataset. For all datasets, the land/sea mask is binary and ocean temperatures covered by sea-ice have been set to -1.8ºC before

regridding (See Section 3 of SI Text). The sea-ice mask provided in HadISST1 is time-dependant.

2. Modeling groups contributing to IPCC database

This analysis relies on Coupled Model Intercomparison Project phase 3 (CMIP3) simulations performed for the Fourth Assessment Report of the Intergovernmental Panel for Climate Change (IPCC AR4). These simulations were made available to the scientific community through the U.S. Dept of Energy's Program for Climate Model Diagnosis and Intercomparison (PCMDI) at Lawrence Livermore National Laboratory (http://www-pcmdi.llnl.gov). In this study, we selected a total of 17 different climate models that have been used to perform both 20CEN *and* A2 experiments (in IPCC terminology, these integrations are referred as "20c3m" and "sresa2", respectively). The number of realizations and the name of modeling group are provided for each model in Table S1. Among these models, eight were designated by Overland and Wang (S3) as capturing key spatial and temporal features of PDO. These models are: CCCma-CGCM3.1 (T47), GFDL-CM2.0, GFDL-CM2.1, MIROC3.2(medres), MIUB/ECHO-G, MRI-CGCM2.3.2, CCSM3.0 and UKMO-HadCM3). More details on the external forcings used in the 20CEN experiments are provided in Santer et al. 2000 (S4).

3. Regridding and masking of data

Each observational dataset and model has a land-sea mask on the original model grid. The projection of a variety of simulated SST anomalies onto multiple observed PDO patterns required that all data share the same horizontal grid and a common land-sea mask. So we regridded data from all observational datasets and model experiments to a common T42 horizontal resolution, in taking appropriately the mask into account. Additionally, in order to mimic the observational

datasets, all regridded SSTs inferior to the threshold of -1.8ºC in the climate simulations are given the -1.8ºC value to represent sea-ice. In the case of HadISST1, the monthly SSTs and the time-dependant sea-ice mask have been regridded first. Then this time-dependant sea-ice mask has been geometrically averaged along the time-axis to provide a time-independent sea-ice mask. To obtain a final land-sea mask common to all datasets, all regridded masks have been averaged geometrically. The final mask excludes any gridpoint that is covered entirely by land in at least one dataset.

4. Details on the calculation of S-PDOP

The official PDO time-series relies on "residual" monthly-mean SST anomalies in the North Pacific region, poleward to 20ºN. The PDO region of consideration in this study extends from 20ºN to 60ºN and from 245ºW to 115ºW. The EOF analysis to obtain S-PDOP accounts for the smaller area weight of the northern latitudes (due to converging meridians) by weighting the gridded SSTs by the square root of the cosine of the latitude. We have then projected the SST anomalies from other observational datasets[11] and from all climate model simulations onto their corresponding S-PDOP. This strategy has been used in the past to produce the official PDO time-series (S5): while HadISST1 data have been used for the period 1900-1993, the PDO time-series has been extended since 1993 using the optimally interpolated SSTs (S6). Our methodology permits to obtain PDO time-series from the simulations, independently of their ability to successfully capture the spatial characteristics associated with PDO. The analysis and interpretation of the spatial PDO pattern obtained from individual IPCC models projections are discussed elsewhere (S7).

5. Statistical tests

5.1. Comparison of unforced and anthropogenically forced trends

We use a Kolmogorov-Smirnov (KS) test to determine whether the trend distributions inferred from the 20CEN (or A2) and CTL experiments differ significantly (S8). The KS test consists at comparing the cumulative distribution A(x) of the 20CEN (or A2) trends with the distribution C(x) of the CTL unforced trends. For the differential warming weteen the PDO and global domains, we test the null hypothesis that $A(x) \geq C(x)$. For the PDO time-series themselves, the null hypothesis is that $A(x) \leq C(x)$. We compute the maximum distance between C(x) and A(x) and the associated one-tailed *p*-value.

5.2. Comparison of observed and unforced trends

The model-derived estimate of the two-tailed 95% confidence interval natural internal variability is calculated as 1.96 x sE, where sE is the standard error of the sampling distribution of the unforced trends. We consider that the observed trend is inconsistent with the simulated response to internal climate variability at the 5% level when its estimated exceeds this 95% confidence interval.

5.3. Calculation of Confidence Intervals for Linear Trends.

The two-tailed statistical significance test used for the least-square linear trend b in the PDO time-series includes an effective sample size adjustment for standard error of slope and critical t-value (S9). The adjustment for temporal autocorrelation assumes a lag-1 autocorrelation structure of the trend residuals, $e(t)$. The lag-1 autocorrelation coefficient of $e(t)$ is used to compute an effective sample size, n_e, and to adjust s_b, the standard error

of b. Strong temporal autocorrelation of $e(t)$ results in $n_e << n$ (the actual number of time samples) and inflates s_b.

6. Sensitivity experiments

6.1. Sensitivity of observed PDO to observational uncertainties

The analyses conducted with the three observational datasets show little sensitivity to observational uncertainties (Table S2, Fig S1). For instance, in all cases, S-PDOP$_1$ is predominantly negative and the observed PDO$_1$ is characterized by a negative trend. Interestingly, the amplitude of this trend over the period 1900-2006 (-0.67 ± 0.4 for ERSST2, -0.76±0.4 for HadISST1, and -1.1 ± 0.4 ºC/century fro ERSST3) is proportional to the spatial average of S-PDOP$_1$ (-0.16, -0.17, and -0.21ºC, respectively). Using definition 2 always succeeds at detrending the PDO$_2$ index (see Table S2), and the difference existing between PDO$_2$ and PDO$_1$ always correlates with the globally averaged SST anomalies, whatever the observational dataset employed. As with the HadISST1 dataset, the differential rate of warming between between 1900 and the beginning of the 60's estimated using the ERSST datasets is faster in the PDO region than globally. The gap between those temperatures shrinks rapidly after 1965 and the difference time-series between PDO$_2$ and PDO$_3$ fluctuates accordingly. Finally, the PDO region once again warms more than the globe starting around the last PDO shift in 1977.

6.2. Sensitivity of the simulated PDO to model screening and weighting

The results presented in the main manuscript are inferred from the eight SELEC climate models (S3). Each model has been given the same, independently of its number of realizations. We tested the sensitivity of the results using two sets of models (using either 8 or 17 models), and two model weighting options (equally-weighted, or weighted as a

function of the number of realizations). Results provided in Table S3 show that the results are not very sensitive to those processing options.

6.3. Sensitivity of observed PDO to the base period

Correlations between various paleo-reconstructions of the PDO (S10-S14) are good over the 20th century. However, they are inconsistent prior that time, suggesting large uncertainties regarding past PDO variability (S15). Using 5000 years of control runs of pure internal climate variability (i.e. in absence of any external forcings), Hunt (S16) found a wide range of possible temporal variability in the PDO (including short period fluctuations, quasi-periodic fluctuations, multidecadal persistence of one regime, and both rapid and slow transitions between regimes). But in their study, only one spatial PDO pattern that is based on the entire record has been used. Here, we investigated the stability of the S-PDOP pattern over time using the dataset with the longest record (ERSST3). For each definition, we determine S-PDOP using 12 different overlapping 50-years base periods (1857-1906, 1867-1916,.., 1957-2006 and the additional 1900-1993). Fig S3A displays the pattern correlations obtained with the first base period (1857-1906). $SPDO_3$ is the least sensitive to the base period used. The variability in the S-PDOP is the most pronounced when definition 1 is used. Fig S3B shows that the trend in PDO_1 over the period 1900-2006 varies greatly with the base period chosen and is proportional to the spatial average of the corresponding S-$PDOP_1$ eigenvectors. This indicates once again the influence of projecting a slowly-evolving warming onto a negative S-$PDOP_1$.

6.4. Sensitivity of the projected future PDO to the based period used to estimate S-PDOP

For each definition, we have projected the future A2 SSTs residuals onto ERSST3-based S-PDOPs calculated from three non-overlapping base periods (1857-1906, 1907-1956, and 1957-2006). The trends vary between -3.8 and -8.0°C/century for PDO_1, -1.7 and -

2.3 °C/century for PDO_2 and -0.9 and -1.3°C/century for PDO_3 (Table S4). This illustrates again that the trends in PDO times-series are sensitive to the base period in definition 1 and relatively insensitive to the base period in definition 3. The use of definition 3 leads to a more stationary S-PDOP pattern and stable PDO indices.

Captions for Figures in Supporting Text

Figure S1: As Fig. 1 but using the ERSST3 dataset.

Figure S2: As Fig. 6 but for the period 1978-1999.

Figure S3: A. For each definition, centered spatial pattern correlation between the S-PDOP based on different overlapping 50-years periods (indicated on the x-axis) with S-PDOP based on the first period (1857-1906). B. Scatter plots between the PDO_1 trends over the period 1900-2006 (y-axis) and the spatial average of the corresponding $S\text{-}PDOP_1$ eigenvectors (x-axis). Each circle represents a different overlapping 50-years period represented in A.

Figure S4: A. Multi-ensemble average of SST trends over the period 1900-1999 (in ºC/decade) using the SELEC models (called hereafter signal). B. Standard deviation of the trends across models (called hereafter noise), C. Signal-to-noise ratio. Regions with a ratio above +2 or below -2 show strong consistency across models. D., E., and F.: Same as A., B. and C. for the period 2001-2099.

Captions for Tables in Supporting Text

Table S1: CMIP3 climate models and their number of 20CEN and A2 realizations. In bold are the eight selected models (3) as able to simulate the variability of 20th century North Pacific SST reasonably well. The asterisk indicates that the model includes some representation of solar and volcanic effect on climate.

Table S2: Statistics on observed S-PDOPs and observed PDOs. Trend significance at the 10%, 5% and 1% levels is indicated by one, two or three asterisks, respectively.

Table S3: Trends in the muti-model ensemble average PDO for two sets of models (the SELEC models or the 17 available models) and for two weighting options (the "equally-weighted" option gives the same weight to each model while in the "weighted" option, the weight of a model is commensurate to the number of realizations). Trend significance at the 10%, 5% and 1% levels is indicated by one, two or three asterisks, respectively.

Table S4: Trends in the muti-model ensemble average PDO using for the SELEC models, the "equally-weighted" option and three different base periods.

Table S1

	20CEN	A2	Modeling groups
CCCma-CGCM3.1 (T47)	**5**	**5**	Canadian Centre for Climate Modelling and Analysis, Canada
GFDL-CM2.0*	**3**	**1**	Geophysical Fluid Dynamics Laboratory, USA
GFDL-CM2.1*	**3**	**1**	Geophysical Fluid Dynamics Laboratory, USA
MIROC3.2(medres)*	**3**	**3**	Center for Climate System Research, National Institute for Environmental Studies, and Frontier Research Center for Global Change, Japan
MIUB/ECHO-G*	**5**	**3**	Meteorological Institute of the University of Bonn, Meteorological Research Institue of the Korean Meteorological Agency, and Model and Data group, Germany/Korea
MRI-CGCM2.3.2*	**5**	**5**	Meteorological Research Institute
CCSM3.0*	**8**	**4**	National Center for Atmospheric Research, USA
UKMO-HadCM3*	**1**	**1**	United Kingdom Meteorological Office Hadley Centre for Climate Prediction and Research, UK
BCCR-BCM2.0	1	1	Bjerknes Center for Climate Research, Norway
CNRM-CM3	1	1	Météo-France / Centre National de Recherhces Météorologiques, France
CSIRO-Mk3.0	3	1	Commonwealth Scientific and Industrial Research Organization (CSIRO) Atmospheric Research, Australia
GISS_ER*	9	1	Goddard Institute for Space Studies, USA
INM-CM3.0	1	1	Institute for Numerical Mathematics, Russia
IPSL_CM4	1	1	Institute Pierre Simon Laplace, France
ECHAM5/MPI-OM	3	3	Max-Planck Institute for Meteorology, Germany
PCM*	4	4	National Center for Atmospheric Research, USA
UKMO-HadGEM1	1	1	United Kingdom Meteorological Office Hadley Centre for Climate Prediction and Research, UK
Selection	**33**	**23**	
All models	57	37	

Table S2

	spatial average (°C)			trend over 1900-2005 (°C/century)			correlation with official PDO		
	S-PDOP1	S-PDOP2	S-PDOP3	PDO1	PDO2	PDO3	PDO1	PDO2	PDO3
HadISST1	-0.17	-0.15	0	-0.76±0.43*	0.17±0.45	0.37±0.44	0.872	0.929	0.899
ERSST2	-0.16	-0.15	0	-0.67±0.44	0.15±0.45	0.04±0.44	0.824	0.905	0.905
ERSST3	-0.21	-0.16	0	-1.14±0.45**	-0.09±0.45	-0.12±0.44	0.704	0.883	0.896

Table S3

models	dataset	20CEN trend			A2 trend		
		PDO1	PDO2	PDO3	PDO1	PDO2	PDO3
SELEC models	HadISST1	-0.36±0.16**	0.49±0.13***	0.39±0.15**	-6.12±0.39***	-2.00±0.22***	-1.18±0.20***
Equally-weighted	ERSST2	-0.27±0.15*	0.45±0.13***	0.36±0.14**	-5.32±0.34***	-1.88±0.21***	-1.18±0.19***
	ERSST3	-0.45±0.15***	0.45±0.12***	0.36±0.14**	-6.17±0.41***	-1.88±0.21***	-1.15±0.19***
SELEC models	HadISST1	-0.52±0.19**	0.38±0.15**	0.36±0.16**	-5.82±0.32***	-1.72±0.21***	-0.94±0.22***
Weighted	ERSST2	-0.40±0.17**	0.37±0.14**	0.34±0.14**	-5.02±0.28***	-1.60±0.20***	-0.94±0.20***
	ERSST3	-0.60±0.18***	0.36±0.14**	0.34±0.15**	-5.88±0.32***	-1.61±0.20***	-0.92±020***
ALL models	HadISST1	-0.23±0.16	0.51±0.12***	0.39±0.13***	-5.50±0.45***	-1.44±0.15***	-0.73±0.13***
Equally-weighted	ERSST2	-0.16±0.14	0.47±0.11***	0.36±0.12***	-4.72±0.37***	-1.32±0.14***	-0.72±0.12***
	ERSST3	-0.31±0.15*	0.47±0.11***	0.35±0.12***	-5.58±0.50***	-1.33±0.14***	-0.70±0.12***
ALL models	HadISST1	-0.22±0.16	0.52±0.11***	0.43±0.13***	-5.30±0.33***	-1.31±0.15***	-0.58±0.16***
Weighted	ERSST2	-0.15±0.14	0.48±0.11***	0.39±0.12***	-4.54±0.29***	-1.20±0.14***	-0.58±0.14***
	ERSST3	-0.31±0.14**	0.48±0.11***	0.39±0.12***	-5.40±0.36***	-1.22±0.14***	-0.57±0.14***

Table S4

models	Base period	20CEN trend			A2 trend		
		PDO1	PDO2	PDO3	PDO1	PDO2	PDO3
SELEC models	1857-1906	-0.71±0.18	0.53±0.14	0.42±0.17	-7.98±0.55	-2.33±0.24	-1.26±0.21
Equally-weighted	1907-1956	-0.45±0.14	0.43±0.12	0.34±0.14	-5.99±0.41	-1.76±0.20	-1.11±0.18
ERSST3	1957-2006	-0.05±0.16	0.45±0.15	0.34±0.17	-3.79±0.27	-1.72±0.22	-0.94±0.20

Supporting References

S1. Smith, TM, Reynolds RW (2004) Improved extended reconstruction of SST (1854-1997). *J. Clim* 17:2466–2477.

S2. Rayner NA, Brohan P, Parker DE, Folland CK, Kennedy J, Vanicek M, Ansell T, Tett SFB (2005) Improved analyses of changes and uncertainties in sea surface temperature measured *in situ* since the mid nineteenth century. *J Clim* 19:446–469.

S3. Overland JE, Wang M (2007) Future Climate of the North Pacific Ocean. *Eos, Transactions Am Geoph Union*, 88:178–182.

S4. Santer BD, Wigley TML, Gleckler PJ, Bonfils C, Wehner MF, *et al*. (2006) Forced and unforced ocean temperature changes in Atlantic and Pacific tropical cyclogenesis regions. *Proc Natl Acad Sci* 103:13905–13910.

S5. Mantua N, Hare S, Zhang Y, Wallace J, Francis R (1997) A Pacific interdecadal oscillation with impacts on salmon production. *Bull Am Met Soc* 58:1069–1079.

S6. Reynolds RW, Smith TM (1995) A High-Resolution Global Sea Surface Temperature Climatology. *J Clim* 16:1571–1583.

S7. Bond NA, Overland JE, Wang M (2006) IPCC Model Projections of North Pacific Climate Variability. *Eos Trans. AGU, 87*(52), Fall Meet Suppl, Abstract OS24C-07.

S8. Press, W. H., B. P. Flannery, S. A. Teukolsky, and W. T. Vetterling, 1992: "Kolmogorov-Smirnov Test." in *Numerical Recipes in FORTRAN: The Art of Scientific Computing*, 2nd ed. Cambridge, England: Cambridge University Press, pp. 617–620.

S9. Santer BD, Wigley TML, Boyle JS, Gaffen DJ, Hnilo JJ, Nychka D, Parker DE, Taylor KE (2000) Statistical significance of trends and trend differences in layer-average atmospheric temperature time series *J Geophys Res* 105:7337–7356.

S10. Biondi F, Gershunov A, Cayan DR (2001) North Pacific decadal climate variability since AD 1661. *J Clim* 14:5–10.

S11. D'Arrigo R, Villalba R, Wiles G (2001) Tree-ring estimates of Pacific decadal climate variability. *Clim Dyn* 18:219–224.

S12. Gedalof Z, Smith DJ (2001) Interdecadal climate variability and regime scale shifts in Pacific North America. *Geophys Res Lett* 28:1515–1518.

S13. MacDonald GM, Case RA (2005) Variations in the Pacific Oscillation over the past millennium. *Geophys Res Lett* 32, L08703, DOI 10.1029/2005GL022478.

S14. D'Arrigo R, Wilson R (2006) On the Asian expression of the PDO. *Int J Climatol* 26:1607–1617.

S15. Shen C, Wang WC, Gong W, Hoa Z (2006) A Pacific Decadal Oscillation record since 1470 AD reconstructed from proxy data of summer rainfall over eastern China. *Geophys Res Lett* 33L03702, doi:10.1029/2005GLO24804.

S16. Hunt BG (2008) Secular variation of the Pacific Decadal Oscillation, the North Pacific Oscillation and climatic jumps in a multi-millennial simulation. *Clim Dyn* 30:467–483.

Fig. S1

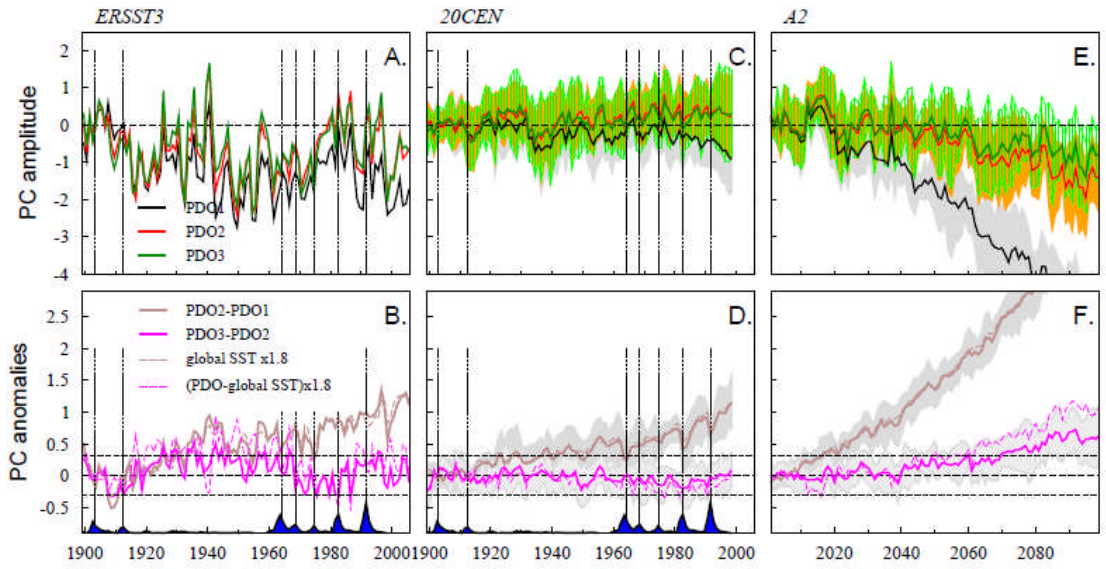
ERSST3
20CEN
A2
A.
C.
E.
B.
D.
F.
PC amplitude
PC anomalies
PDO1
PDO2
PDO3
PDO2-PDO1
PDO3-PDO2
global SST x1.8
(PDO-global SST)x1.8
1900 1920 1940 1960 1980 2000
2020 2040 2060 2080

Fig. S2

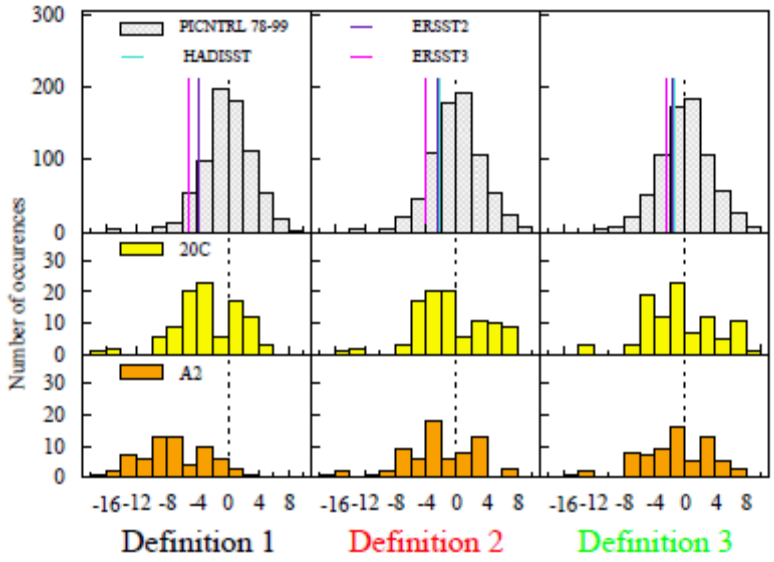
PICNTRL 78-99
HADISST
ERSST2
ERSST3
20C
A2
Number of occurences
-16 -12 -8 -4 0 4 8
Definition 1
Definition 2
Definition 3

Fig. S3

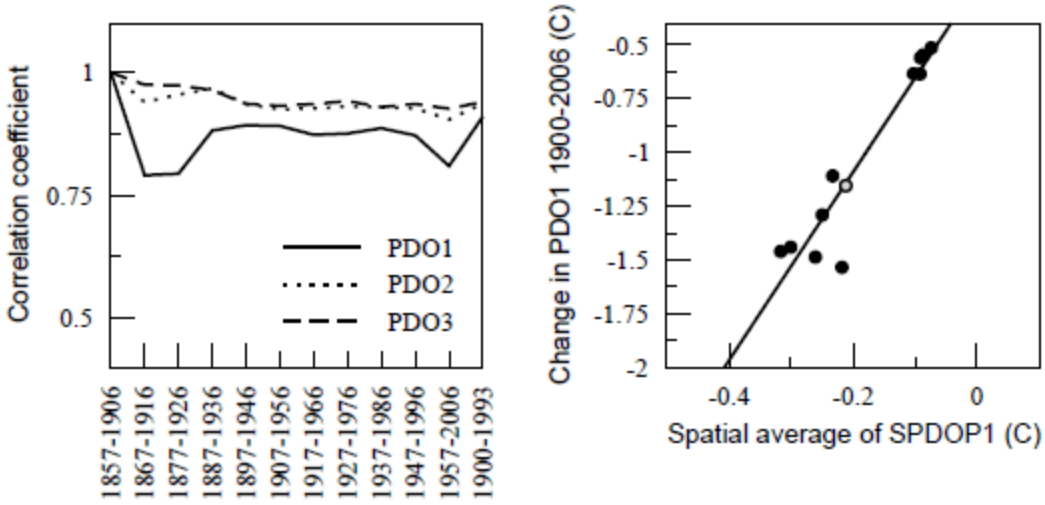
Correlation coefficient
1
0.75
0.5
PDO1
PDO2
PDO3
1857-1906
1867-1916
1877-1926
1887-1936
1897-1946
1907-1956
1917-1966
1927-1976
1937-1986
1947-1996
1957-2006
1900-1993
Change in PDO1 1900-2006 (C)
-0.5
-0.75
-1
-1.25
-1.5
-1.75
-2
-0.4
-0.2
0
Spatial average of SPDOP1 (C)

Fig. S4

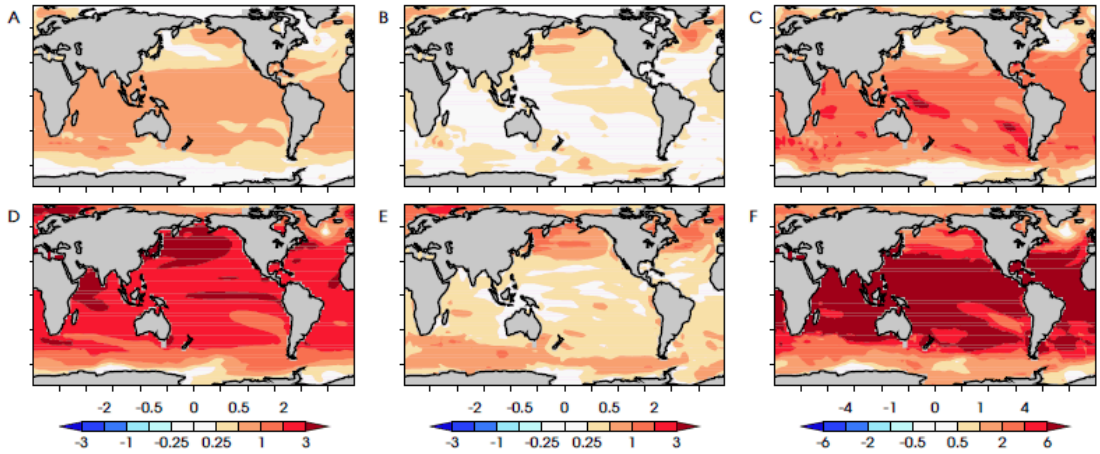
A
B
C
D
E
F
-2 -0.5 0 0.5 2
-3 -1 -0.25 0.25 1 3
-2 -0.5 0 0.5 2
-3 -1 -0.25 0.25 1 3
-4 -1 0 1 4
-6 -2 -0.5 0.5 2 6